Conf-8710159--7

DYNAMICS AND STRUCTURE OF ENERGETIC DISPLACEMENT CASCADES

R. S. Averback and T. Diaz de la Rubia*
Department of Materials Science
University of Illinois at Urbana-Champaign
Urbana, IL 61801

and

*Department of Physics
SUNY at Albany
Albany, NY 12222

R. Benedek**
Materials Science Division
Argonne National Laboratory
Argonne, IL 60439

CONF-8710159--7

DE88 005803

December 1987

DISCLAIMER

INVITED PAPER presented at the International Conference on Atomic Collisions in Solids, Okayama, Japan, October 12-16, 1987 and to be published in Nuclear Instruments and Methods.

**Work supported by the U.S. Department of Energy, BES-Materials Sciences, under Contract #W-31-109-ENG-38.

Dynamics and Structure of Energetic Displacement Cascades

R. S. Averback and T. Diaz de la Rubia*
Department of Materials Science
University of Illinois at Urbana-Champaign
Urbana, Il. 61801
and
*Department of Physics
SUNY at Albany
Albany, N.Y. 12222

R. Benedek
Materials Science Division
Argonne National Laboratory
Argonne, Il. 60439

Abstract

This paper summarizes recent progress in the understanding of energetic displacement cascades and the primary state of damage in metals. On the theoretical side, the availability of supercomputers has greatly enhanced our ability to simulate cascades by molecular dynamics. Recent application of this simulation technique to Cu and Ni provides new insight into the dynamics of cascade processes. On the experimental side, new data on ion beam mixing and in situ electron microscopy studies of ion damage at low temperatures reveal the role of the thermodynamic properties of the material on cascade dynamics and structure.

1. Historical Background

The nature of energetic displacement cascades has been of interest to physicists and materials scientists since the birth of atomic energy over four decades ago. By the end of the 1950's, most of the fundamental processes occurring in cascades were at least hypothesized, if not actually observed.

The original concept of a displacement cascade appears to be due to Brinkman who suggested that as the energy of a projectile in a solid falls below a critical level, its mean free path between collisions approaches the interatomic spacing, thereby resulting in the production of a high density of displaced atoms (1). In this picture, vacancies are localized in the core of the cascade and self-interstitial atoms (SIA's) reside on the periphery. It was later (1958) suggested by Seeger (2) that SIA's are transported from the cascade region as "dynamic crowdions," i.e., replacement collision sequences (RCS's) along close-packed directions, and that efficient separation of SIA's and vacancies could be achieved by this mechanism. The concept of RCS's was further elucidated the following year by the Brookhaven group in one of the first applications of molecular dynamics (MD) computer simulation (3). The role of thermal spikes in cascades was first discussed in detail by Seitz and by Seitz and Koehler (4). A thermal spike results from the conversion of the kinetic energy of the primary recoil atom into heat in the localized region of the cascade. Its existence requires that the energy be partitioned among the atoms in the cascade region such that local equilibrium is approached before the spike dissipates. Seitz and Koehler also considered the possibility of enhanced diffusion within the cascade resulting from the thermal spike, but they estimated that for a 500 eV recoil event the diffusion was negligible (4). Later, Vineyard showed that thermally activated processes are, in fact, of significance in higher energy cascades (5). Thus, many of the key features of displacement cascades were anticipated before ≈ 1960. In the decades that followed, work has been directed towards establishing the relative importance of each of these processes on the various properties of the cascade. In this paper, some of the progress achieved in the last few years will be summarized. This includes new theoretical studies using molecular dynamic computer simulation and experimental studies of ion beam mixing and "cascade collapse." A brief comment on the possible influence of the electronic system on cascade dynamics is presented in the conclusion.

2. Cascade Dynamics and Structure

The traditional approaches to the problem of cascade dynamics have

alternated between ignoring the many-body aspects of the problem, e.g, invoking the binary collision approximation and linearized transport equations (6-8), or ignoring the higher energy collisions and assuming that quasi-local equilibrium is rapidly approached such that classical heat flow and chemical rate theory can be applied (5,9). This dichotomy of views emphasizes either the "collisional" phase or the "thermal spike" phase of the cascade. It has been difficult to reconcile these approaches by analytical means. The most adequate method currently available for treating the cascade problem is molecular dynamics (MD) computer simulation. MD is, of course, a rather brute-force approach, but for a number of inhomogeneous many-body problems, it is the only practical recourse.

The pioneering studies of the Brookhaven group helped elucidate the defect production process in low energy (< 400 eV) events. It was found that RCS's propagate along close-packed directions and that this mechanism efficiently separates SIA's from vacancies. Subsequently, Vineyard (10) used the MD results to calculate isotherms in the cascade under the assumption of energy equipartition. This early work was severely limited by the computational resources available at that time. To extend the calculations to higher energies, hybrid schemes that combine binary collision simulations with either MD or Monte-Carlo procedures were developed, for example, by Beeler and coworkers. Purely MD studies, however, were limited to energies below a few hundred eV's until quite recently.

Using more powerful computers, Guinan and Kinney performed MD simulations on W at energies from 25 eV to ≈ 5 keV (11). Their results demonstrated that point defects created during the collisional phase of the cascade undergo extensive diffusion with the possibility of recombination during the thermal spike and that this process becomes more pronounced with increasing recoil energy. This behavior provides a plausible explanation for the experimental observation that defect production efficiency decreases with increasing recoil energy (12,13).

Recently, the present authors have performed MD simulations of cascades in Cu and Ni at energies up to 5 keV (14), and the results will be summarized here. These are the highest energies, in reduced units, that have been treated by MD. Cu interactions were represented in the simulations by the Gibson II

Born-Mayer potential (3) and Ni interactions by a composite of potentials due to Erginsoy (short-range) (15) and Johnson (long-range) (16). Some important features of cascades are illustrated in Fig. 1, which shows the lattice sites on which atomic replacements occurred in a 5 keV event in Cu. Also shown in the figure are the final locations of SIA's. The majority of replacements occur in the central core of the cascade although a few of the replacements form trails that lead to SIA's. Whereas all the SIA's lie outside the central core, the vacancies, shown in Fig. 1b (open circles), form a compact depleted zone. Although these qualitative features are similar to those predicted by Seeger already in 1958 (2) and in more recent binary collision computer simulations (7,17), a quantitative understanding of defect production, clustering, and atomic mixing is only now emerging from a detailed analysis of MD simulations.

The dense cloud of replacements in the core of the cascade indicates that most of the atomic rearrangements within a cascade are not simply a byproduct of the defect production process (via RCS's). Analysis of simulations for Cu reveals that a process akin to melting occurs, and is responsible for extensive atomic mixing. This is illustrated by plotting a projection of the atomic positions in a cross sectional slab of thickness $a_o/2$ (a_o is the lattice parameter) near the center of the cascade at various instants of time. An example (based on the event illustrated in Fig. 1) corresponding to a time t=I.1 ps, is shown in Fig.2. (The event was initiated at t=0 by imparting a 5 keV kinetic energy to one of the lattice atoms in an otherwise perfect crystal; this corresponds to T=0 K). We observe a relatively well defined disordered zone embedded in a somewhat distorted crystalline matrix. Examination of similar snapshots reveals the presence of a disordered zone before the collisional phase has ended. This disordered zone initially grows to some maximum size and then shrinks as recrystallization occurs at its periphery. Recrystallization is complete at t=8 ps. Radial pair distribution functions, g(r), for the atoms in the disordered zone were constructed to provide a more quantitative characterization. In Fig. 3, we show these pair distribution functions at t=1.1 ps and 3.4 ps as well as a simulation for liquid Cu (18). Most striking is the disappearence of the (200) crystalline peak in g(r) at 3.6 Å. We note that the lifetime of the disordered region is

a few ps., i.e., ≈ 20-50 lattice vibration periods; it is at least plausible that a quasi-equilibrium state could be established in this interval. We have performed further analyses to characterize the thermal spike in more detail. In Figs. 4a and 4b are plotted the temperatures (assuming 3/2 k_BT = average kinetic energy/atom) and atomic densities as functions of distance from the center of the cascade (taken as the center of mass of the instantaneous vacancy distribution) at different times in the cascade evolution. At early times, ≈ 0.25 ps, the average temperature (which perhaps is not yet well defined) in the center of the cascade, r < 10 Å is ≈ 5000 K, and the temperature gradient outside this central core is ≈ 300 K/Å. The initial cooling rate in the center of the cascade is ≈ 10^{15} K/s . At 1.4 ps, the temperature begins to fall below the melting temperature of Cu at a position r ≈ 17 Å. It can be seen in Fig. 2b that this radius corresponds closely to the radius of the disordered zone (note, however, the slightly different times).

Fig. 4b shows that the atomic density variation is proportional to the temperature profile. Expansion in the hot central core of the cascade gives rise to a much reduced density, as much as ≈ 15 % at 1.14 ps. It can also be seen that a high-density ridge is formed outside the hot core. We note that this high density is not primarily due to SIA's transported from the center of the cascade by RCS's. Moreover, as the high temperature zone cools, the compression at the cascade periphery relaxes, returning the density to its equilibrium value.

Results of additional analyses are given in Table 1. Here the average temperatures in the cascade at various times are tabulated using two characteristic radii to define the cascade volume, the radii of gyration (R_{gv} and R_{gi}) of the vacancy and SIA distributions. Also listed in Table 1 are the fraction of atoms within R_{gi} that have energies greater than 0.05 eV (f^*_1) and 5.0 eV (f^*_2), which correspond roughly to the fractions of "moving" atoms and atoms with collisional (as opposed to diffusive) trajectories, respectively. We note that the fraction of moving atoms, f^*_1, increases to over 90% in less than 0.2 ps. This is a consequence of the short mean free path of low energy atoms. The time at which all kinetic energies have fallen below 5 eV, which we somewhat arbitrarily define as the end of the collisional phase, occurs

between 0.2 and 0.4 ps. Thus, some overlap occurs between the collisional and thermal spike phases.

3. Atomic Mixing

Although the thermal-spike aspects of cascades, and even the possibility of local melting, have long been recognized, the quantitative consequences of this behavior have been difficult to predict. In Fig. 5, the atomic mixing generated in our 5 keV event in Cu is represented by the mean square displacement per atom,

$$\sum_i [(r_i(t_o,r) - r_i(0,r))^2]/n(r) = 6\langle D_c(r)t_o\rangle, \quad (1)$$

plotted at two instants of time as a function of distance from the center of the cascade. The index i refers to the i^{th} atom belonging initially to a coordination shell containing n(r) atoms at a distance r with respect to the center of the cascade. The two times correspond approximately to the end of the collisional phase and the end of the thermal spike. It is evident that only a small fraction of the mixing occurs during the collisional phase and that the vast majority of mixing can be attributed to the thermal spike. It is also noteworthy that the absolute magnitude of the total mixing ($\langle D_c t\rangle$, normalized to the damage energy) obtained from simulation is 16 $Å^5$/eV which is in excellent agreement with the experimental value of 20 $Å^5$/eV (19). In view of the rather schematic interatomic force model employed in the simulations, this close agreement may be fortuitous, however it does provide some evidence that the basic physics is correct. Peak et al. proposed a model of ion-beam mixing based on liquid-state diffusion (20); using experimental values of tracer impurity diffusivities and the cascade cooling rate obtained from the MD simulations, they obtained reasonable agreement with experiment, which gives additional support for the present interpretation.

Atomic mixing was also studied by direct simulation of a "heat spike"

(14). A heat spike was generated by assigning initial kinetic energies to atoms in a local region of the crystallite according to a Maxwellian distribution. The atomic mixing obtained in heat-spike simulations is shown in Fig. 6 for Cu and Ni, plotted as a function of energy density. For values of the energy density in the range expected for a 5 keV Cu or Ni cascade, ≈ 1-2 eV/atom, the agreement between the heat spike simulations, the primary recoil atom simulations and experiment is quite reasonable. Clearly evident in Fig. 6 is a large difference in the mixing between Cu and Ni (both in the simulations and experiment). In light of our present view that atomic mixing occurs primarily in the liquid droplet, it is natural to attribute the differences between results for Cu and Ni to their different melting temperatures. The melting temperature is correlated both to the liquid diffusion coefficient and to the lifetime of the liquid droplet. Another factor that may result in different values of mixing in Cu and Ni is the phonon-electron damping; this possibility will be discussed briefly in the summary.

The importance of thermal spikes in cascade dynamics suggests a direct relationship between the thermochemical properties of metals and cascade effects, and this has been demonstratated by recent ion beam mixing experiments. In Fig.(7) the parameter, $Dt/\Phi F_D$, where $(t/\Phi F_D)^{-1}$ is the rate of damage energy deposition, is shown for several metals; the data show the relationship between the thermal properties of the metal and ion beam mixing (20). The corresponding host metal and the value $Dt/\Phi F_D$ are indicated within the circles. The values of $Dt/\Phi F_D$ represent the average spreading of two or more impurity "marker" atoms during 1 MeV Kr irradiation at 10 K. The ordinate, F_D^2, is related to the energy density, or cascade "temperature", characteristic of cascades in the metal. Metals with high atomic numbers tend to have high energy densities. The abscissa is a measure of the inverse cohesive energy (which can be taken to be inversely proportional to the melting temperature). It can be seen in Fig.(7) that for fixed cohesive energy, the mixing parameter increases with increasing energy density, and for fixed energy density, the mixing parameter increases with decreasing cohesive energy. These dependences are quite strong, with variations of over an order

of magnitude. As mentioned above, the mixing parameter in Cu is a factor of 3-4 greater than that in Ni.

In other experimental studies, Johnson and co-workers demonstrated that chemical driving forces can also play a significant role in ion beam mixing (21). By combining Vineyard's equation for the number of thermally activated jumps that occur in a cascade (5),

$$\eta = A[\varepsilon^2/KCQ^2] \qquad (2)$$

and the Darken relation for chemical interdiffusion (22),

$$D = D_o(1 - 2\Delta H_{mix}/kT), \qquad (3)$$

Johnson et al. derived the expression

$$4Dt/\Phi = K_1\varepsilon^2/\rho^{5/3}(\Delta H_{coh})^2\ [1 + K_2(\Delta H_{mix}/\Delta H_{coh})]\ , \qquad (4)$$

for ion beam mixing in diffusion couples (21). The terms $\Phi, \varepsilon, \rho, \Delta H_{mix}$, ΔH_{coh}, K and C are the ion dose, energy density per unit path length of the ion, atomic density, heat of mixing, cohesive energy, thermal conductivity and specific heat, respectively. In deriving eq. (4), Johnson assumed proportionality between the activation enthalpy for the diffusion process, Q in Vineyard's equation, and the cohesive energy of the material. K_1 and K_2 in eq. (4) are phenomenological constants. The substantial success of this model can be seen in Fig. (8), which shows the mixing of 4d transition elements with either Au or Pt (23). This work demonstrates (i) the importance of thermochemical properties for diffusion in cascades, and (ii) that the energies that characterize atomic mixing processes must be less than about 1 eV/atom, since otherwise ΔH_{mix} would be too small to have any influence (21).

4. Defect Production and Clustering

Local melting in the cascade also has important implications for defect production. Fig. 1a shows that only those SIA's that are transported beyond the boundaries of the melt zone by RCS's survive eventual recombination. With regard to total defect production, the simulations yielded an average value of 12 Frenkel pairs for four 5-keV events. This value corresponds to an efficiency of 0.2 with respect to the modified Kinchin-Pease relation, in reasonable agreement with experiment (12). According to our present picture,

this low efficiency is attributed to the "absorption" (recombination) of those SIA's that don't escape through the boundary of the melt. It follows from this picture that defect production efficiency should decrease with increasing energy since the dimensions of the cascade, and of the melt zone, increase with increasing energy. This behavior is consistent with experimental observation (12). At sufficiently high energies, on the other hand, a cascade splits into subcascades. It is natural to hypothesize that that these subcascades are associated with distinct droplets formed during the thermal spike. In this regime, the efficiency is expected to become energy-independent, which is indeed observed experimentally (12).

The simulations provide information regarding the local arrangement of SIA's and vacancies in their nascent cascades. The distribution of RCS lengths for simulated 3 and 5 keV cascades in Cu are shown in Fig 9. (Only those RCS's leading to the final positions of the SIA's are included in this distribution). Although most surviving SIA's escape the region of the melt by RCS's, they can still undergo extensive diffusive motion before coming to rest. Since attractive elastic interactions exist between SIA's, some interstitial clustering occurs. Clusters containing ≈ 3-5 SIA's in nascent cascades have been observed experimentally by diffuse x-ray scattering measurements on a number of pure metals following fast neutron irradiation at 6 K (24).

Owing to the loss of SIA's by RCS's, the interior of the cascade contains an excess of vacancies, or depleted zone, after the melt resolidifies. On the basis of the highly clustered arrangements of vacancies observed in Field-Ion Microscope studies of cascades, Seidman et al conclude that the locations of vacancies within depleted zones in W have little correlation with the locations on which they were produced. In some cases, voids and dislocation loops were observed (25). In the past few years, studies of the dynamic collapse of depleted zones into dislocation loops and stacking-fault tetrahedra at low temperatures have provided additional insight into the primary state of damage (26,27). These studies have employed in-situ ion irradiation (in a TEM) of thin film specimens at temperatures below stage I. Some results of such studies are summarized in Table 2, which lists the dislocation loop yields for a variety of ion-target combinations. A

comparison of these yields with the ion-beam induced mixing results, Fig.(7), strongly suggests that these two phenonmena are related, both depending on the energy density in the cascade and the melting temperature of the metal.

Seidman has suggested that the rearrangement of vacancies within the cascade derives from the precipitation of vacancy clusters in the highly supersaturated depleted zone and their growth during the thermal spike (25). Another possible mechanism for cascade collapse is the thermotransport of vacancies towards the center of the cascade and SIA's toward the periphery, driven by the the steep temperature gradient (28,29). Both of these mechanisms require high vacancy mobility during the thermal spike. Our present simulation results suggest an alternative, but related, explanation. Since the crystal is destroyed within the melt zone, vacancies lose their identity in this region. As solidification begins, from outside in, the crystal regrows with few frozen-in vacancies. As the solidification proceeds, however, the density fluctuations in the melt increase (the fraction of missing atoms increases) until finally vacancies begin to freeze out. In this way, vacancies are driven to higher concentrations at the center of the cascade. We suggest that this regrowth mechanism might be crucial for establishing the conditions under which collapse can occur. We note also that vacancy collapse in Cu has not been observed experimentally at energies less than 10 keV, and therefore MD studies at somewhat higher energies than in the present work would be of great interest to see whether collapse can be simulated directly.

Concluding Remarks

It has been our intention to show that thermal spikes play an important role in many properties of energetic displacement cascades. A quantitative understanding of this role is beginning to emerge from molecular dynamics computer simulations. These simulations should become increasingly valuable as more realistic interatomic potentials are employed and as parallel-processing capabilities of advanced computers are exploited more fully, enabling higher PKA energies to be treated. One of the approximations in the simulations is the neglect of phonon-electron coupling. A simple remedy is to include a viscous-damping term to simulate electronic excitations; such a procedure is,

in fact, standard practice in binary collision simulations (7). This treatment, is based on the assumption that the electronic mean-free path is too large for equilibration between the electron and phonon systems to occur within the excited cascade region. On the other hand, we note that the mean-free path in liquid Cu at its melting point is about 45 Å (37), which is only slightly larger than typical cascade dimensions. Moreover, considerably smaller mean-free paths exist in other liquid metals. Thus, phonon-electron coupling may lead to stronger damping of the thermal spike in some metals than would be predicted by viscous-damping models. The negative result of a thermionic emission experiment on stainless steel (38), however, deserves mention in this context. Nevertheless, we believe the issue of phonon-electron coupling deserves further study.

Acknowledgments

We are grateful to Prof. C.P. Flynn for bringing to our attention the possible role of phonon-electron coupling in cascades. We also thank Prof. D.N. Seidman for numerous discussions. Our MD computer code was adapted from one developed by Prof. J.R Beeler, Jr. The MD simulations were performed on the CRAY-2 at the MFE computer center under a grant from the U.S Department of Energy, Basic Energy Sciences. One of us (TDR) is grateful to SUNY-Albany for a Presidential Graduate Fellowship. This work was supported by the U.S. Department of Energy, Basic Energy Sciences under grants DE-AC02-76ER01198 and W-31-109-ENG-38, at the University of Illinois and Argonne National Laboratory, respectively.

References

1. J.A. Brinkman, J. Appl. Phys. **25** (1954) 961; Am. J. Phys. **24** (1956) 246.
2. A. Seeger, Proc. 2nd UN Intnl Conf. on Peaceful Uses of Atomic Energy, Proc. Conf. Geneva, 1958, Vol 6 (IAEC,Vienna,1958) p. 250 .
3. J.B. Gibson, A.N. Goland, M. Milgram and G.H. Vineyard, Phys. Rev. **120** (1960) 1229.
4. F. Seitz and J.S. Koehler, Solid State Physics **2**, eds. F. Seitz and D. Turnbull, (Academic Press, New York, 1956) p. 307.
5. G.H. Vineyard, Radiat. Eff. **29** (1976) 245
6. P. Sigmund, Radiat. Eff. **1** (1969) 15.
7. M.T. Robinson and I.M. Torrens, Phys. Rev. B **9** (1974) 5008.
8. P. Sigmund and A. Gras-Marti, Nucl. Instr. and Meth. **182/183** (1981) 25.
9. J.B. Sanders, Rad. Eff. **51** (1980) 43.
10. G. Vineyard, Disc. Farad. Soc. **31**, (1961) 7.
11. M.W. Guinan and J.H. Kinney, J. Nucl. Mater. **103/104** (1981) 1319.
12. R.S. Averback, R. Benedek and K.L. Merkle, Phys. Rev. B **18**, (1978) 4156.
13. P. Jung, J. Nucl. Mater., **117** (1983) 70.
14. T.D. de la Rubia, R.S. Averback, R. Benedek and W.E. King, Phys. Rev. Lett. 59 (1987) 1930; and T.D. de la Rubia, R.S. Averback and R. Benedek, unpublished.
15. C. Erginsoy, G.H. Vineyard and A. Englert, Phys. Rev. 133 (1964) A595
16. R.A. Johnson, Phys. Rev. **145** (1966) 423.
17. a. H. Heinisch, J. Nucl. Mater. **103/104** (1981) 1325.
    b. R. Benedek, J Appl. Phys. **52** (1981) 5557.
18. S. Foiles, Phys. Rev. **B 32** (1985) 3409.
19. R.S.Averback, D. Peak and L.J. Thompson, Appl. Phys. **A 39** (1986) 59.
20. S-.J.Kim, M-A. Nicolet, R.S. Averback and D. Peak, Phys. Rev. in press; and D. Peak, unpublished.
21. W.L. Johnson, Y.T. Cheng, M. Van Rossum and M-A. Nicolet, Nucl. Instr. and Meth., **B7/8** (1985) 657.
22. See, e.g., P. Shewmon, *Diffusion in Solids*, (McGraw Hill, N.Y., 1963) p. 126.
23. T.W. Workman, Y.T. Cheng, W.L. Johnson and M-A. Nicolet, Appl. Phys. Lett.

50 (1987) 1486.

24. D. Grasse, B.v. Guerard and J. Peisl, J. Nucl. Mater.,**120** (1984) 304.
25. D. Pramanik and D.N. Seidman, Nucl Instr. and Meth., **209/210** (1983) 453.
26. C.A. English and M.L. Jenkins, Mater. Science Forum,15-18 (1987) 1003.
27. M.A. Kirk, I.M. Robertson, M.L. Jenkins, C.A. English, T.J. Black and J.S. Vetrano, J. Nucl. Mater. **149** (1987) 21.
28. V.I. Protasov and V.G. Chudinov, Rad. Eff. **66** (1982) 1.
29. V.G. Kapinos and P.A. Platonov, Rad. Eff. **103** (1987) 45.
30. K. Haga, A. Baily, W.E. King, K.L. Merkle and M Meshii, 7th Int. Conf. on High Voltage Electron Microscopy, ed. R.M. Fisher et al. U.C. Report LBL-16031 1983, p. 139.
31. K.L. Merkle and W.E. King, unpublished.
32. T.J. Black, M.L. Jenkins, C.A. English and M.A. Kirk, Proc. R. Soc. Lond. **A 409** (1987) 177.
33. M.L. Jenkins, C.A English and B.L. Eyre, Phil. Mag. **38** (1978) 97.
34. I.M. Robertson, M.A. Kirk and W.E. King, Scripta Met. 18 (1984) 317.
35. C.A. English, B.L. Eyre, A.F. Bartlett, and H.N.G. Wadley, Phil Mag. **35** (1977) 533.
36. M.A. Kirk, I.M. Robertson, J.S. Vetrano, M.L. Jenkins, L.Funk, unpublished.
37. T.E. Faber, in *Physics of Metals 1. Electrons*, ed. J.M. Ziman (Cambridge at the University Press, Cambridge, 1969) p. 284.
38. F. Thum and W.O. Hofer, Surface Sci. **90** (1979) 331.

Figure Captions

1. a) View of final SIA locations (o) produced in a simulated 5 keV event in Cu, and the sites on which replacements occurred (x), and b) view of both the final SIA (o) and vacancy (o) locations. The primary recoil direction corresponded to polar and azimuthal angles of 39.1° and 22.5°, respectively, and the PKA site was about 20 Å from the center of mass of the final vacancy distribution. The computational cell, whose boundaries are indicated by the solid lines, is tilted 15° about the (110) axis.

2. Projection of a (100) cross sectional slab of thickness $a_o/2$, near the center of a 5 keV cascade at t = 1.10 ps.

3. Radial pair distribution functions, g(r), corresponding to the disordered zones at t= 1.10 and 3.84 ps. Results for liquid Cu (18) are shown for comparison.

4. a) Temperature profile at three instants of time for a 5 keV event in Cu. b) Density profile corresponding to the same cascade as in (a).

5. The mean square displacement per atom as a function of distance from the "center" of a 5 keV cascade at t = 1.2 ps and at t = 10.0 ps.

6. Atomic mixing for a "heat spike" simulation in Cu and Ni as a function of energy density. Also indicated are the values of atomic mixing for a simulated 5 keV primary recoil event in Cu and values obtained from experiment.

7. Dependence of the ion beam mixing parameter, $Dt/\Phi F_D$, on cohesive energy and energy density for several metals. (Ref.20)

8. Correlation between ion beam mixing and $\Delta H_{mix}/\Delta H_{coh}$ for various diffusion

couples. Irradiation was at 77 K with 600 keV Kr. (Ref. 23)

9. Distribution of "final" RCS lengths corresponding to simulated events at 3 and 5 kev in Cu.

Table 1. Characteristics of a 5 keV displacement cascade in Cu

time (ps)	R_{gi} (Å)	$\langle T(R_{gi})\rangle$ (eV/at)	$\langle T(R_{gi})\rangle$ (K)	f^*_1	f^*_2	R_{gv} (Å)	$\langle T(R_{gv})\rangle$ (eV/at)	$\langle T(R_{gv})\rangle$ (K)
0.048	11.9			.47	.24	8.54		
0.105	16.14	1.53	5,909	.85	.083	13.22	1.62	6,255
0.165	19.46	1.02	3,936	.94	.011	14.73	1.25	4,813
0.250	21.9	0.64	2,459	.97	.002	15.03	0.88	3,417
0.437	24.1	0.39	1,508	.91	.000	16.90	0.54	2,164
1.410	23.9	0.25	978	.83	.000	17.26	0.39	1,507
3.470	21.24	0.22	864	.87	.000	14.62	0.28	1,076
4.860	17.1	0.175	676	.83	.000	11.86	0.23	890
6.240	18.4	0.155	600	.84	.000	9.53	0.22	844

Table 2. Yields for Cascade Collapse

Metal	Ion	Temp(K)	Yield	Ref.	$Dt/\Phi F_D$[a]
Ag	100-keV Kr	10	1.0	30	60-90
Au	140-keV Kr	10	1.0	31	80-140
Cu_3Au	50-keV Kr	30	0.5	32	20-40[b]
Fe	80-keV Fe	300	0.0	33	6-7
Fe	50 keV Fe	30	0.0	34	
Mo	60 keV Mo	300	0.16	35	6-10
Ni	50-keV Ni	30	0.08	36	8-10

[a] Data of Kim et al (20)

[b] Value for Cu

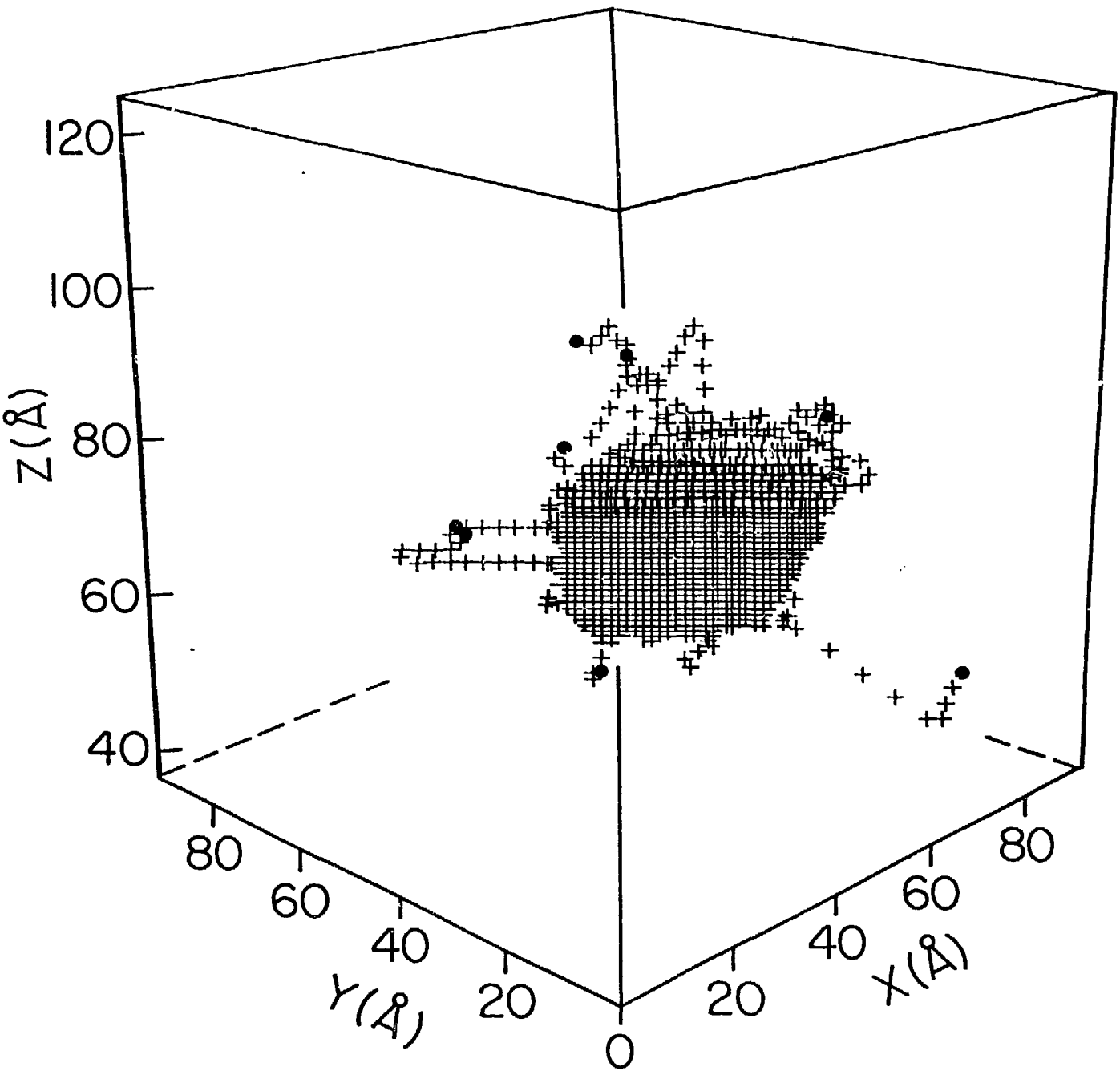
120
100
80
60
40
Z(Å)
80
60
40
20
0
Y(Å)
20
40
60
80
X(Å)

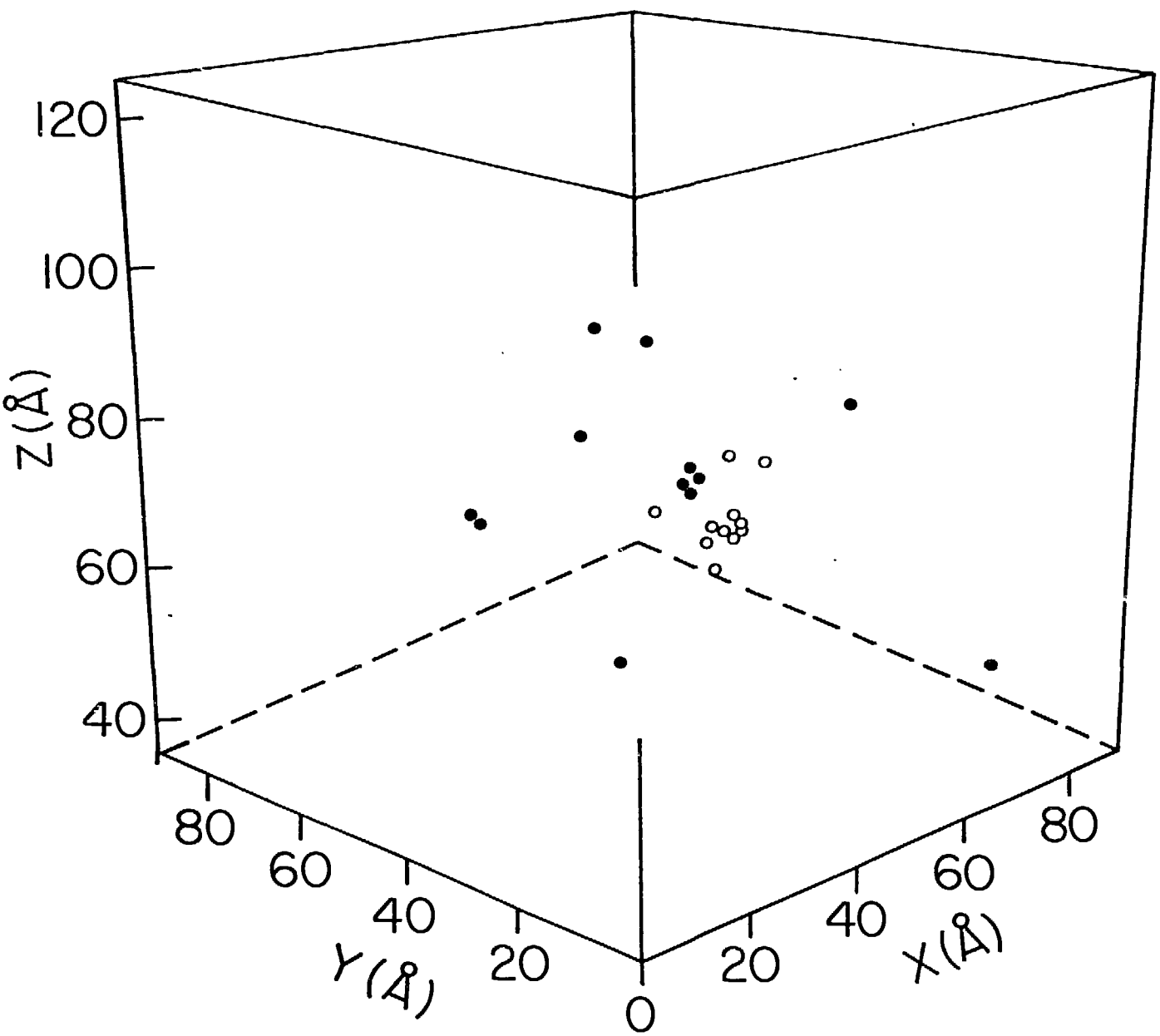
120
100
80
60
40
Z(Å)
80
60
40
20
0
Y(Å)
0
20
40
60
80
X(Å)

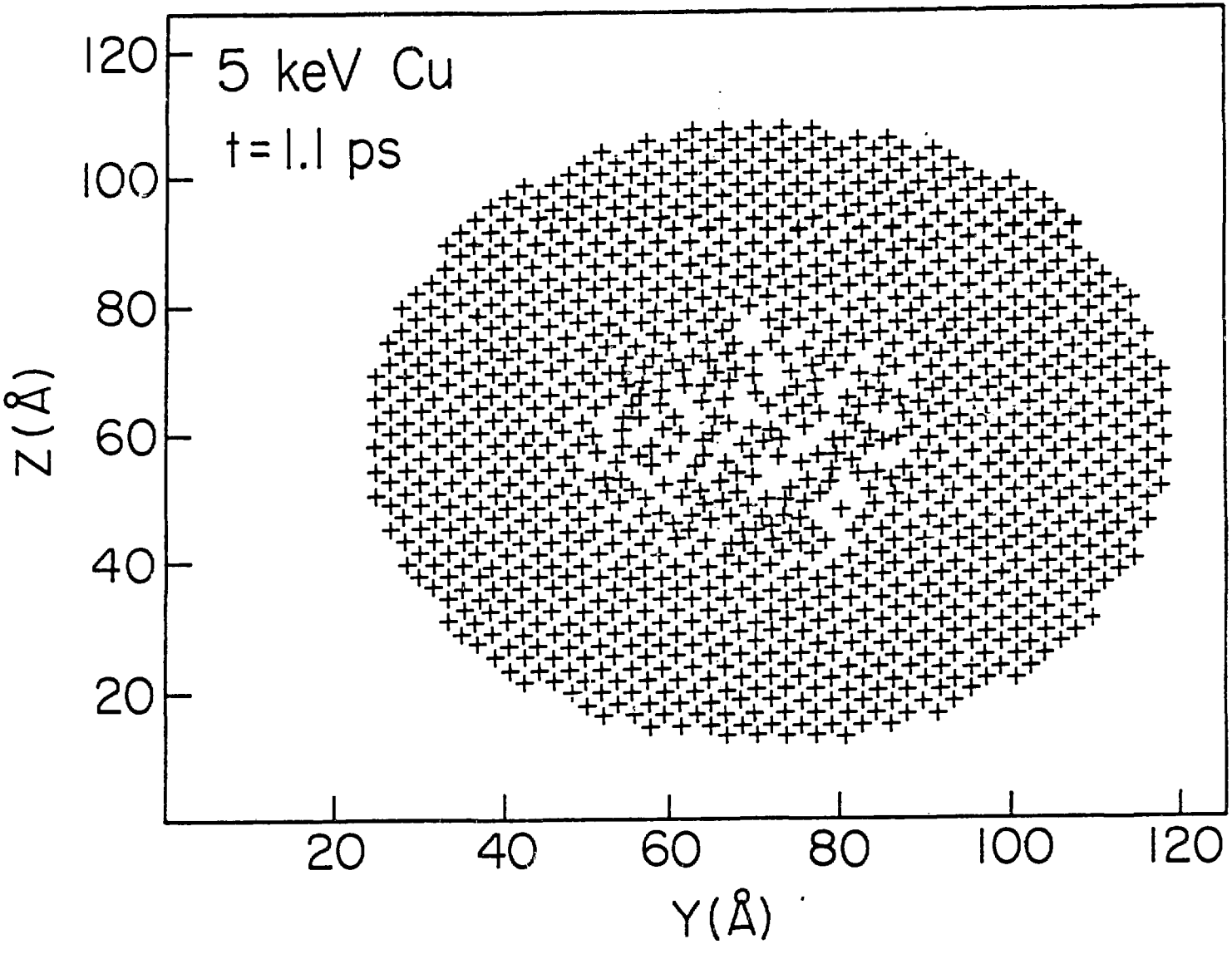
5 keV Cu
t=1.1 ps
120
100
80
60
40
20
Z(Å)
20
40
60
80
100
120
Y(Å)

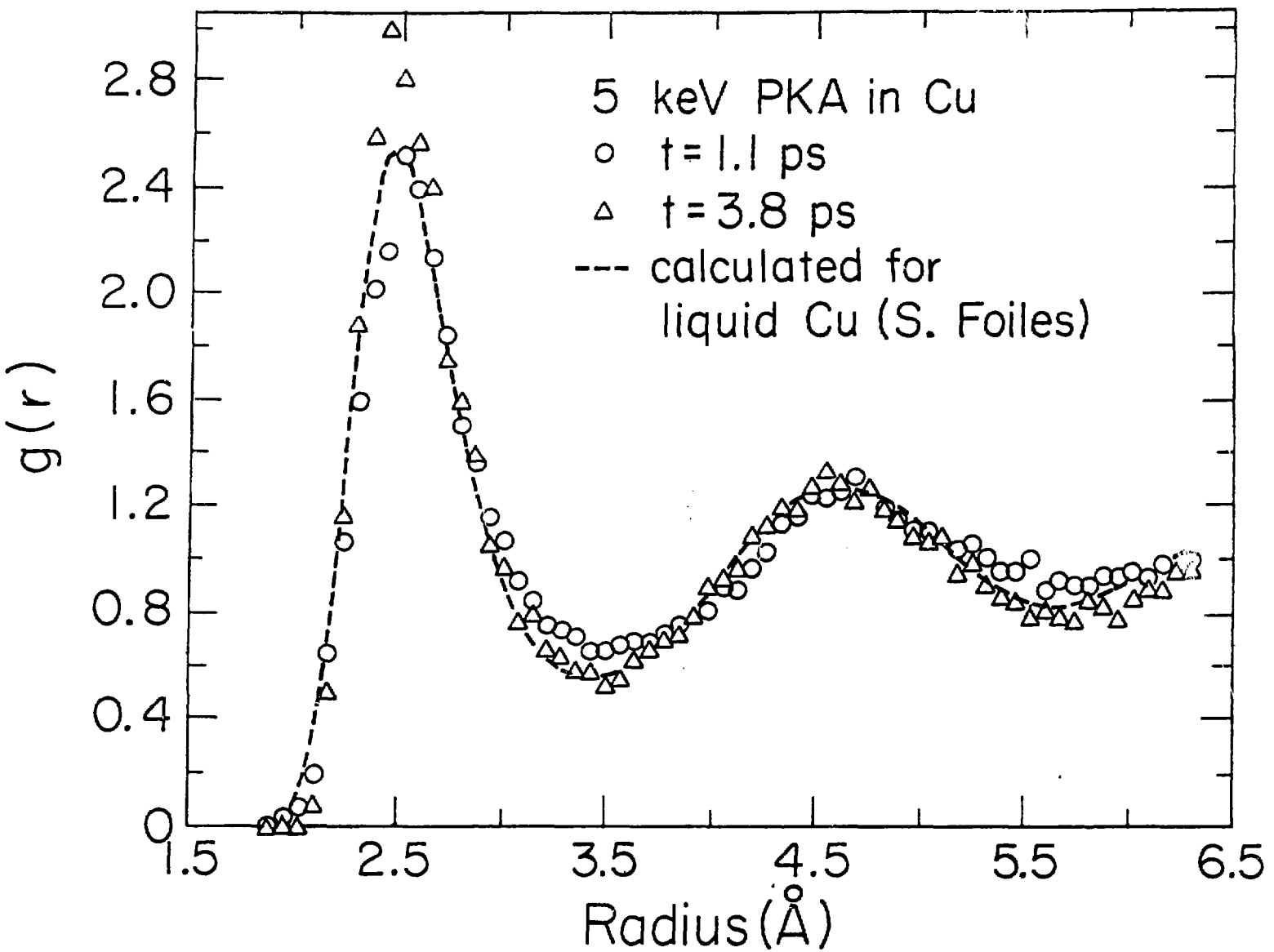
5 keV PKA in Cu
t = 1.1 ps
t = 3.8 ps
--- calculated for
liquid Cu (S. Foiles)
g(r)
2.8
2.4
2.0
1.6
1.2
0.8
0.4
0
1.5
2.5
3.5
4.5
5.5
6.5
Radius (Å)

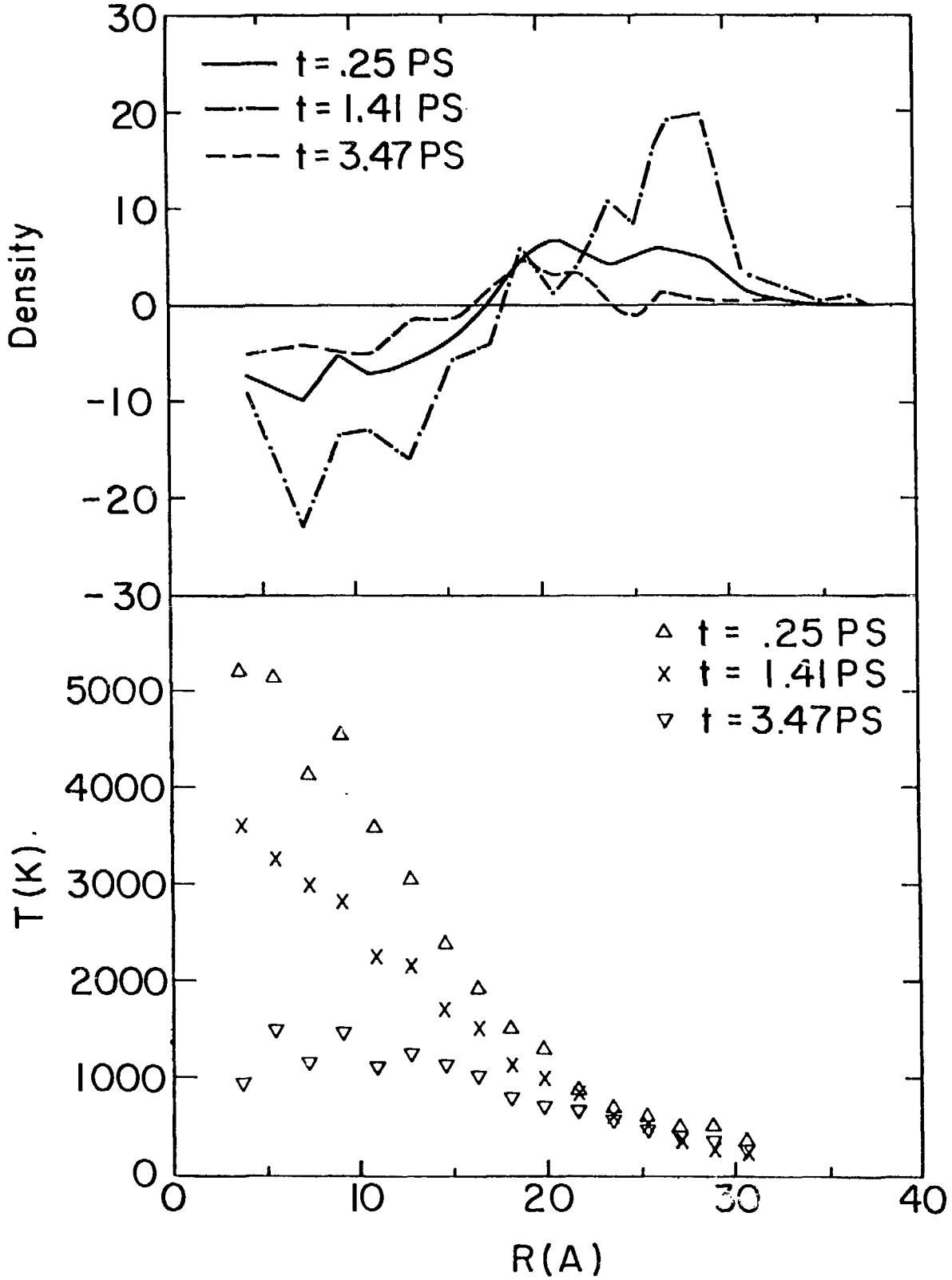
t = .25 PS
t = 1.41 PS
t = 3.47 PS
Density
30
20
10
0
-10
-20
-30
t = .25 PS
t = 1.41 PS
t = 3.47 PS
T(K).
5000
4000
3000
2000
1000
0
0
10
20
30
40
R(A)

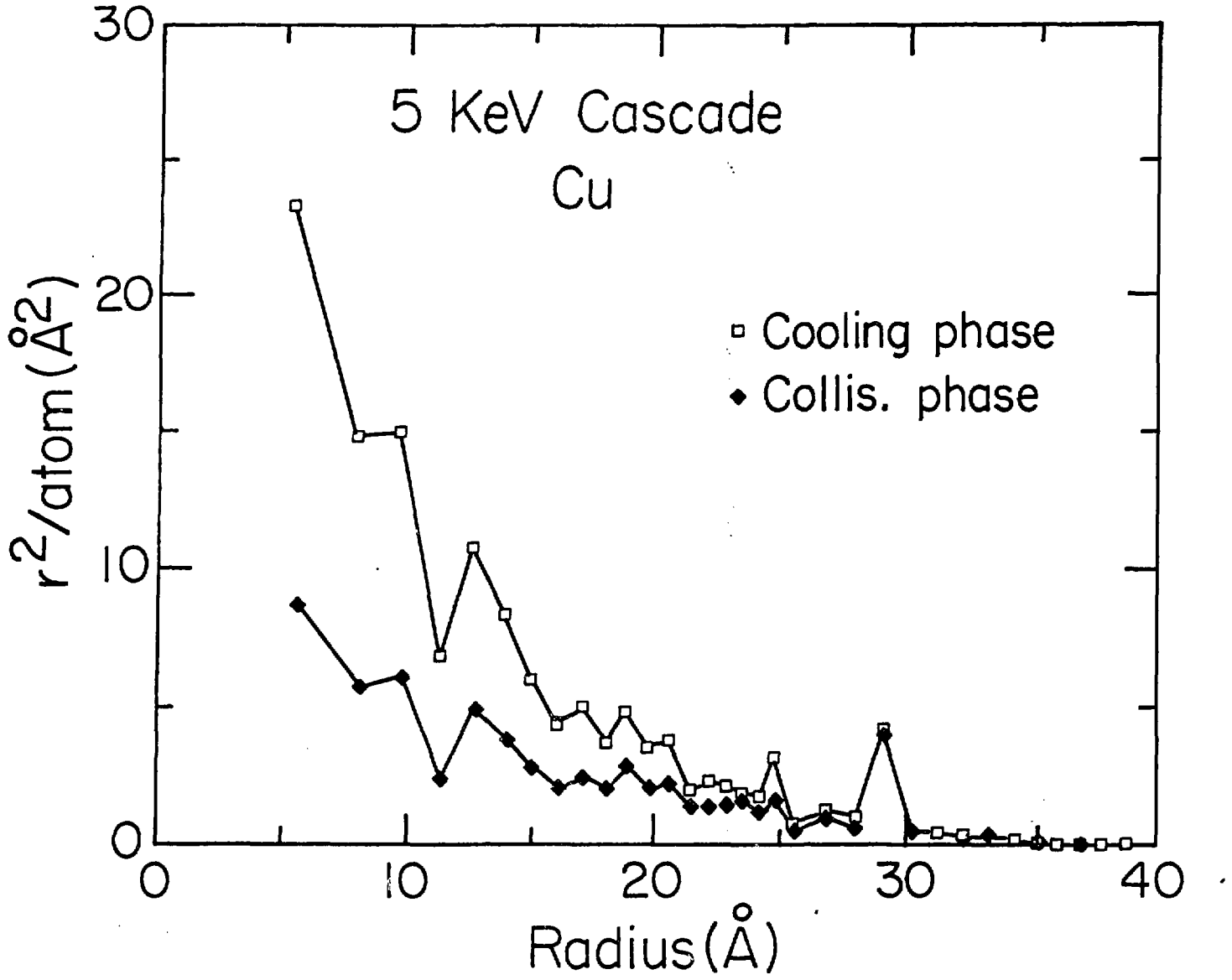
5 KeV Cascade
Cu
Cooling phase
Collis. phase
r²/atom (Å²)
Radius (Å)
0
10
20
30
40

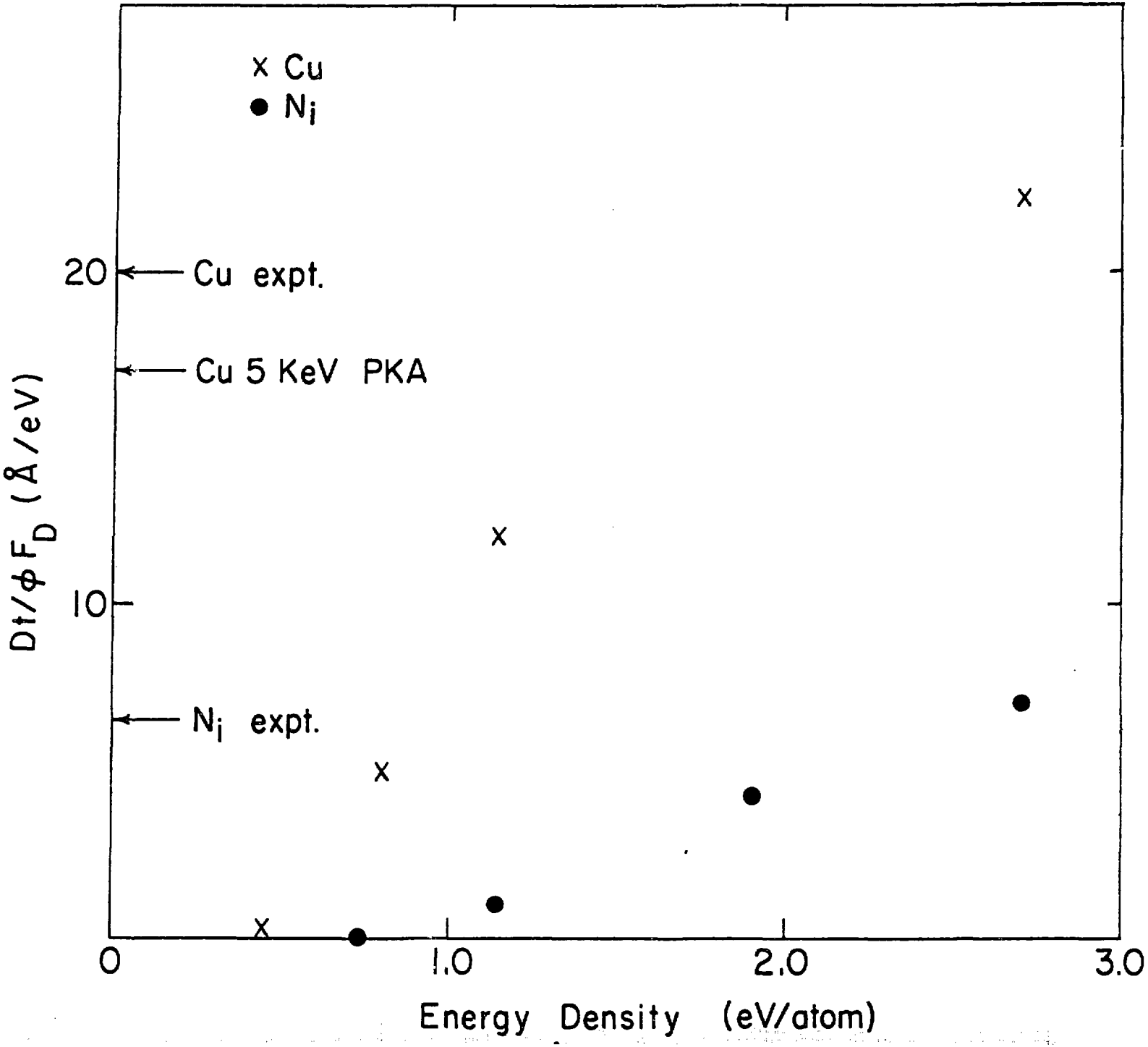
x Cu
● Ni
20
Cu expt.
Cu 5 KeV PKA
10
Ni expt.
Dt/φF_D (Å/eV)
0
1.0
2.0
3.0
Energy Density (eV/atom)

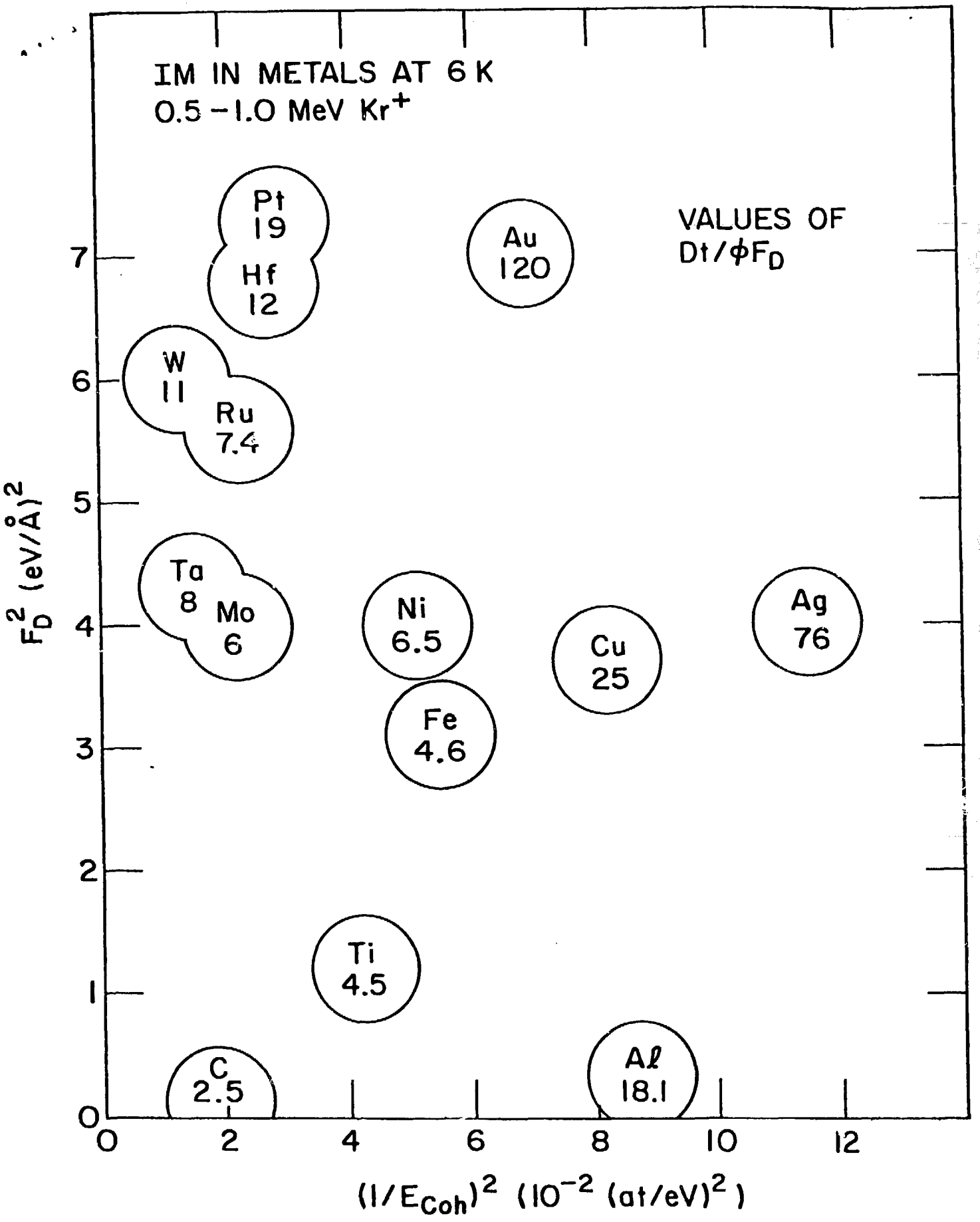
IM IN METALS AT 6 K
0.5 – 1.0 MeV Kr+
VALUES OF
Dt/φF_D
Pt
19
Hf
12
Au
120
W
11
Ru
7.4
Ta
8
Mo
6
Ni
6.5
Cu
25
Ag
76
Fe
4.6
Ti
4.5
C
2.5
Al
18.1
F_D^2 (eV/Å)^2
(1/E_Coh)^2 (10^-2 (at/eV)^2)
0
1
2
3
4
5
6
7
0
2
4
6
8
10
12

2½"

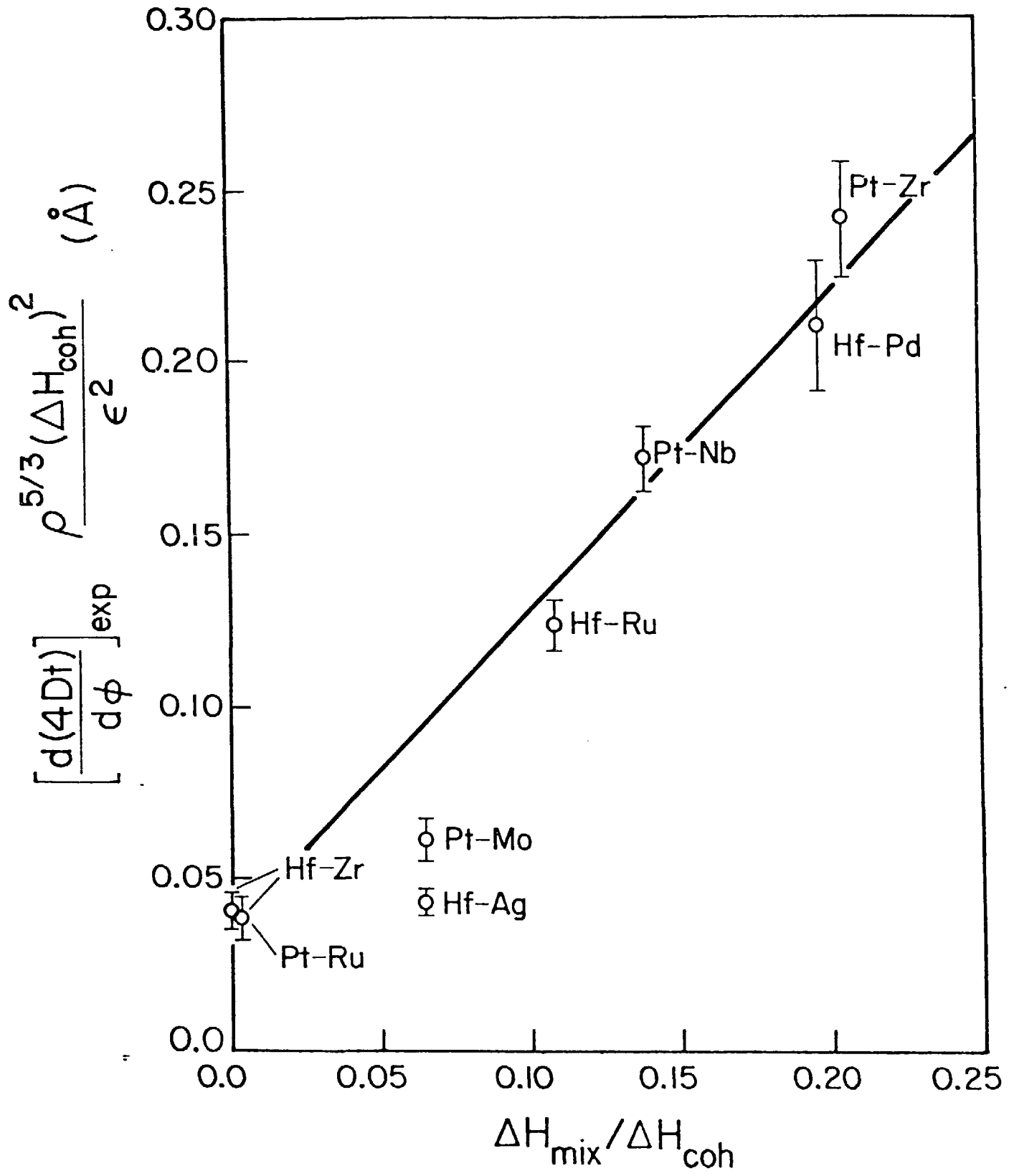
0.30
0.25
0.20
0.15
0.10
0.05
0.0
0.0
0.05
0.10
0.15
0.20
0.25
$\left[\frac{d(4Dt)}{d\phi}\right]_{exp} \frac{\rho^{5/3}(\Delta H_{coh})^2}{\epsilon^2}$ (Å)
$\Delta H_{mix}/\Delta H_{coh}$
Pt-Zr
Hf-Pd
Pt-Nb
Hf-Ru
Pt-Mo
Hf-Ag
Hf-Zr
Pt-Ru

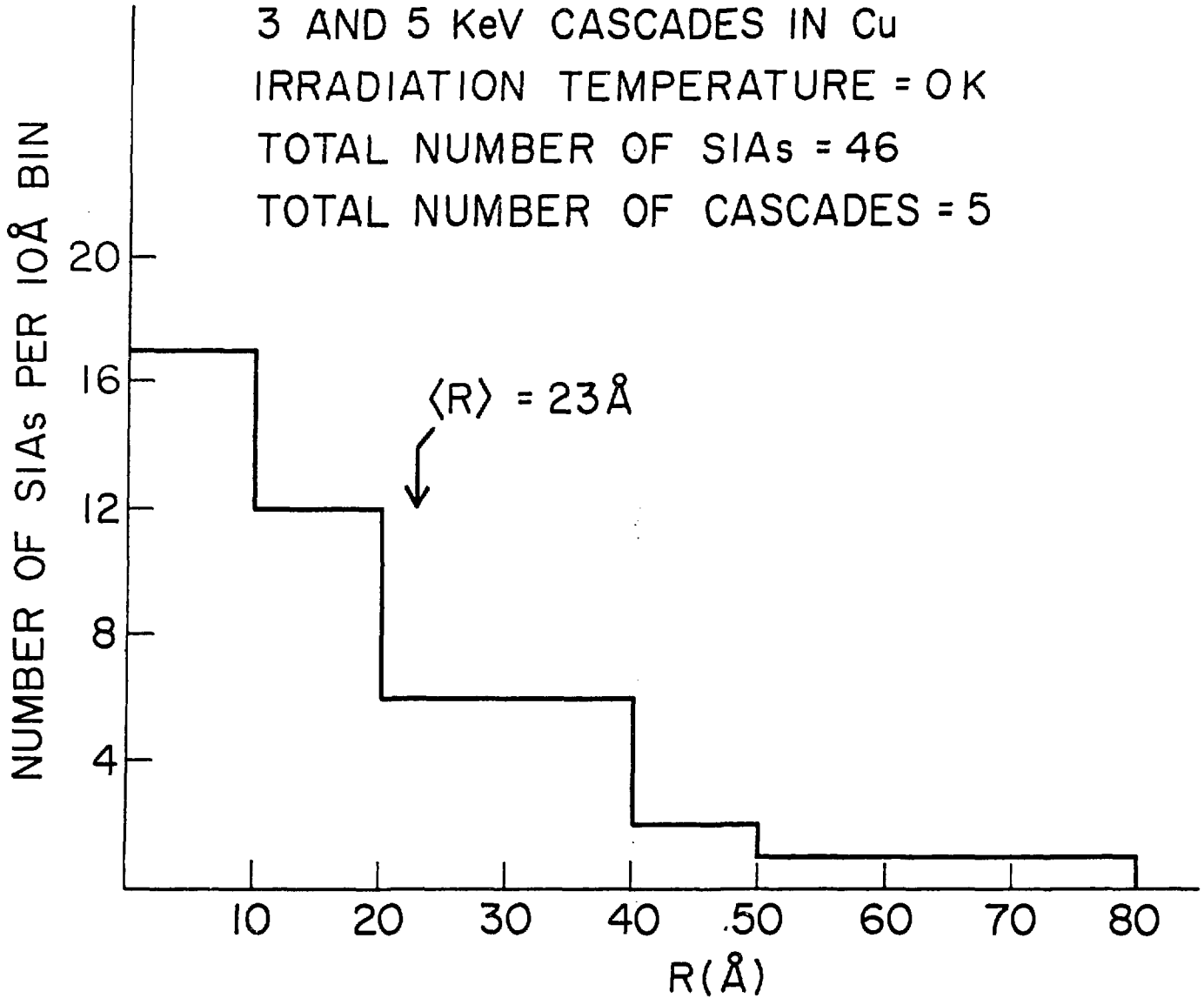
3 AND 5 KeV CASCADES IN Cu
IRRADIATION TEMPERATURE = 0 K
TOTAL NUMBER OF SIAs = 46
TOTAL NUMBER OF CASCADES = 5
NUMBER OF SIAs PER 10Å BIN
20
16
12
8
4
⟨R⟩ = 23Å
10
20
30
40
50
60
70
80
R(Å)